International Communications in Heat and Mass Transfer 126 (2021) 105393

Contents lists available at ScienceDirect

International Communications in Heat and Mass Transfer

journal homepage: www.elsevier.com/locate/ichmt

Quantitative evaluation of effects of coupled temperature elevation, thermal damage, and enlarged porosity on nanoparticle migration in tumors during magnetic nanoparticle hyperthermia

Manpreet Singh, Ronghui Ma, Liang Zhu *

Department of Mechanical Engineering, University of Maryland Baltimore County, Baltimore, MD 21250, USA

ARTICLE INFO

Keywords:
Bioheat transfer
Magnetic nanoparticle hyperthermia
Nanoparticle migration in tumors
Thermal damage
Diffusion enhancement

ABSTRACT

Using simulation to accurately design a heating protocol in magnetic nanoparticle hyperthermia relies on not only the initial nanoparticle distribution, but also the dynamic particle migration during heating. A coupled theoretical framework consisting of nanoparticle migration in a porous medium model and temperature elevation in a heat transfer model was developed to evaluate possible nanoparticle redistribution during local heating. Five generated tumor models from microcomputed tomography (microCT) with nanoparticle deposition were used to predict temperature elevations and assess local thermal damage when each tumor was subject to an alternating magnetic field. Local thermal damage further changed the interstitial structure in the tumor, resulting in enhancements in porosity and diffusion coefficient to promote nanoparticle diffusion to low concentration regions. The distribution volumes of nanoparticles in the highest concentration range reduced after heating, while those in the lower concentration ranges increased. After heating, the total nanoparticle distribution volume defined as the tumor volume occupied by nanoparticles was 21% bigger than that before the heating. The theoretical predictions of nanoparticle migration trend agree well with experimental results of microCT scan analyses. It is concluded that thermal damage induced enhancement in nanoparticle diffusion may be one of the mechanisms to explain nanoparticle migration during magnetic nanoparticle hyperthermia. Results from this study may suggest a feasibility of enhancing nanoparticle dispersion from injection sites using deliberate thermal damage.

1. Introduction

Magnetic nanoparticle hyperthermia (MNH) is a minimally invasive and effective approach for cancer treatment due to its unique capability of confining energy generation in tumors with minimal collateral damage to healthy tissue [1,2]. Magnetic nanoparticles delivered to tumors can induce localized heating when agitated by an alternating magnetic field [3], mainly due to Neel's relaxation and/or Brownian motion of nanoparticles. After a hyperthermia treatment, nanoparticles may remain inside the tissue for weeks or months. Removal of nanoparticles from the body is primarily handled via renal and hepatic/biliary pathways.

Previous studies have demonstrated that iron particle size, particle coating, and magnetic field strength and frequency determine its specific loss power, defined as the energy generated per unit time and per unit mass of iron. However, once the iron nanoparticles are manufactured, the spatial distribution of the particles in tumors dominates the spatial temperature elevation, therefore, it directly affects design of heating protocols to damage tumor cells [4]. If nanoparticle distribution in tumors can be determined before heating, it is feasible to conduct theoretical analyses to simulate temperature elevation history in the tumor, and to determine the required thermal dosage to achieve irreversible thermal damage to targeted tumors. However, current imaging systems in animal and clinical studies may not allow in vivo or in vitro real-time monitoring of particle distribution in tissue. Without experimental data of particle dynamics during heating, most theoretical simulations rely on the assumption that nanoparticle distribution inside tumors remains unchanged during heating.

Experimental studies in the past provided indirect evidence of nanoparticle migration during heating. Using rodents with xenograft prostate cancer tumors, it was noted that on day 4 after injections, 79% of the injected magnetic nanoparticles were still present in the prostate

* Corresponding author at: University of Maryland Baltimore County, 1000 Hilltop Circle, Baltimore, MD 21250, USA.
E-mail address: zliang@umbc.edu (L. Zhu).

https://doi.org/10.1016/j.icheatmasstransfer.2021.105393

Available online 17 June 2021

[5]. Therefore, implementing multiple heating sessions over a course of several weeks after a single intratumoral injection of ferrofluid was explored by researchers to enhance the treatment efficacy [5–10]. Interestingly, those experiments showed a much more uniform temperature elevation in the tumors in later repeated heating sessions [8,10]. The observed change in the distribution of temperature field could be explained by more dispersed nanoparticles in tumors after the initial heating.

However, in most of the previous theoretical simulations to design heating protocols using magnetic nanoparticles, the redistribution of nanoparticles was not modeled. Based on the very small value of the diffusion coefficient of nanoparticles in tumor interstitium [4], those previous studies assumed that the non-uniform nanoparticle distribution in tumors remained unchanged during heating. Designed protocols based on the initial nanoparticle concentration distribution in the tumor may not be accurate to achieve optimal therapeutic outcomes. It is therefore critical to understand how heating in a tumor affects the local nanoparticle distribution and to what extent nanoparticle redistribution influences the temperature elevations in the heating treatment.

Using microcomputed tomography (microCT) as an imaging tool to quantify nanoparticle distribution in PC3 (prostatic cancer) tumors, we have demonstrated different nanoparticle deposition patterns in tumors injected with a commercially available ferrofluid with or without local heating [1,11–13]. Ideally, the same tumor before and after local heating should be scanned to investigate the heat-induced nanoparticle re-distribution [1]. However, lack of access to a microCT capable of imaging life animals led to scans of resected tumors in those studies. Nevertheless, statistically significant differences on the nanoparticle distribution volume in resected tumors were established between a control group without heating and an experimental group with heating. A much larger volume with nanoparticle deposition in tumors with heating was observed than that in tumors without localized heating, suggesting possible nanoparticle redistribution/migration during heating. Although understanding of nanoparticle migration may require real-time imaging tools, cost-effective mathematical simulation provides an alternative method to evaluate how various transport mechanisms influence nanoparticle migration during heating.

Transport of nanoparticles in biological tissues such as tumors is a complicated process that involves nanofluid flowing through tumor interstitial space, advection of nanoparticles in the porous tumor due to lymphatic drainage, diffusion of particles, particle binding to and unbinding from tumor cells, etc. Theoretical simulations of nanoparticle transport have to take into consideration those various mechanisms. Local heating might increase the amount of blood delivered to tumors, promote lymphatic drainage, and modify the interstitial space structure. We hypothesize that the intracellular solutions might be released from dead cells after rupture of cell membranes, if the thermal dosage delivered is sufficient to cause irreversible thermal damage. This would increase the porosity of the tumor, which subsequently facilitates nanoparticle diffusion. Nanoparticle migration in a porous medium might be possible once diffusion overcomes other forces trapping the particles in their initial locations. Nanoparticles originally confined might be able to diffuse to low concentration locations due to the enhanced diffusion coefficient. This hypothesis was tested in a previous study to evaluate nanoparticle diffusion in a spherical tumor subject to local heating in a one-dimensional setting [12]. The dynamic interactions among temperature elevations, thermal damage, and nanoparticle diffusion during magnetic nanoparticle hyperthermia treatment were evaluated via modified tumor porosity and effective diffusion coefficient of nanoparticle concentration in a porous tumor. The simulation results have shown that thermal damage-induced nanoparticle redistribution has increased the nanoparticle distribution volume by 62%. However, the one-dimensional setting of the problem in that study does not fully represent the random and irregular deposition of nanoparticles in a realistic tumor after an intratumoral injection of ferrofluid [1,12]. It is unclear to what extent particle migration might proceed in realistic PC3 tumor models with injected nanoparticles.

In this study, we developed a three-dimensional theoretical model incorporating coupled heat and mass transport in porous tumoral tissue during local magnetic nanoparticle hyperthermia. The model was used to evaluate the extent to which the enhanced nanoparticle diffusion increases nanoparticle distribution volume in PC3 tumors after local heating. The Pennes bioheat equation was used to simulate temperature elevations in a microCT generated tumor model with magnetic nanoparticle deposition during the heating process. The blood perfusion rate, metabolism in tumors, and tumor porosity were coupled with local thermal damage using the Arrhenius integral. Finally, a mass transport equation was implemented to simulate possible diffusion of nanoparticles, providing a dynamic volumetric heat generation rate distribution in the heat transfer simulation. The simulated nanoparticle redistribution was then compared to our previous experimental results of microCT scans of resected tumors with or without heating. To the best of our knowledge, this is the first study to evaluate nanoparticle migration in realistic tumor models with the initial particle concentration distribution obtained through microCT scans.

2. Methods

Experimental procedures of generating a tumor model with nanoparticle concentration distribution were described in a previous study by our group [1]. Briefly, PC3 tumor cells were injected to the left flank of Balb/c Nu/Nu male mice. Once the tumor grew to a size larger than 10 mm in transverse diameter, the mouse was brought to the lab and 0.1 cc of a commercially available ferrofluid (EMG 700, Ferrotec Corporation, Bedford, NH) was injected to the center of the tumor. After the completion of the ferrofluid infusion, the mouse was euthanized and the tumor was resected for microCT scan using a high-resolution microCT system (Skyscan 1172, Micro Phontonics, PA). The obtained microCT images were reconstructed and a tumor model was generated. The grayscale values in individual voxel locations were converted into a volumetric heat generation rate at the voxel location via calibration, described in our previous study [1]. Five tumor models were generated. The generated tumor physical model was then attached to a previously generated mouse body to mimic the situation in the original animal experiments [1,13], as shown in Fig. 1.

It is assumed that both the tumor and mouse body are made of a homogeneous material. The tumor surface is exposed to a free convection environment (h = 3.7–4.8 W/m^{2}K, depending on the size of the tumor, T_{air} = 25 °C). At the bottom surface of the mouse body, a constant temperature of 37 °C is prescribed to mimic the experimental setup where the mouse bottom surface was in contact with a heating pad maintained as 37 °C. The rest of the mouse body surface is subject to a

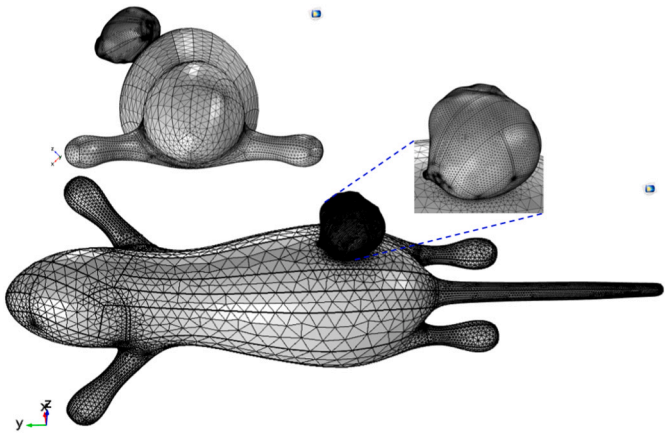

Fig. 1. Top view and side view of the geometry and numerical meshes of a PC3 tumor implanted on the flank of a generated mouse model.

convection environment ($h = 10$ W/m^{2}K, $T_{air} = 25$ °C).

The mathematical model consists of a heat transfer equation and a diffusion equation to describe transient heat transfer and nanoparticle migration processes, respectively, in the generated three-dimensional tumor model during magnetic nanoparticle hyperthermia. Starting with an initially non-uniform concentration of nanoparticles in the tumor, the Pennes bioheat equation [14] is solved for the temperature field that is subsequently used to determine the heat-induced thermal damage. The thermal damage is then translated to an enlarged local tumor porosity. With the modified tumor porosity, the enhanced diffusion coefficient of the nanoparticles is calculated, followed by simulation of nanoparticle concentration using the diffusion equation. As this model employs a linear relationship between the volumetric heat generation rate by the nanoparticles and nanoparticle concentration, the effects of dynamic nanoparticle redistribution on temperature elevations are incorporated in the Pennes bioheat equation throughout the transient heat transfer process. Therefore, the heat and mass transfer equations in this model are fully coupled to describe the dynamic interactions of heating with particle migration. Besides, the model also considers the dynamic responses of blood perfusion rate and metabolism to local heating.

In a three-dimensional Cartesian coordinate, the Pennes bioheat equation [14] for the transient temperature field in the tumor (T_{tumor}) and mouse (T_{mouse}) during magnetic nanoparticle hyperthermia is:

$$\rho_{tumor}c_{tumor}\frac{\partial T_{tumor}}{\partial t} = k_{tumor}\nabla^2 T_{tumor} + \frac{\omega_{tumor,0}}{e^{\Omega}}\rho_b c_b(T_b - T_{tumor}) + \frac{Q'''_{met,tumor,0}}{e^{\Omega}} + Q'''_{MNH} \quad (1)$$

$$\rho_{mouse}c_{mouse}\frac{\partial T_{mouse}}{\partial t} = k_{mouse}\nabla^2 T_{mouse} + \omega_{mouse,0}\rho_b c_b(T_b - T_{mouse}) + Q'''_{met,mouse,0}$$

where ρ is the density, c is the specific heat, and k is the thermal conductivity. Subscripts *tumor*, *mouse*, and *b* denote the tumor region, the mouse body region, and blood, respectively. T_b is the arterial blood temperature prescribed as 37 °C. Subscript *0* represents the initial value of either the blood perfusion rate ω or the volumetric heat generation rate due to metabolism Q'''_{met}. Q'''_{MNH} in Eq. (1) is the volumetric heat generation rate due to the injected magnetic nanoparticles subject to an alternating magnetic field in the tumor region, and its value is proportional to the nanoparticle concentration C in tissue, which is

$$Q'''_{MNH}(x,y,z,t) = 2266.67^{*}C(x,y,z,t) \quad (2)$$

This linear relationship was derived based on experimental data in a previous study by our group [1]. The local thermal damage [15] is quantified by a dimensionless Arrhenius integral Ω:

$$\Omega(x,y,z,t) = A\int_0^t exp\left[-\frac{E_a}{R_u T_{tumor}(x,y,z,\tau)}\right]d\tau \quad (3)$$

where A is the frequency factor (1/s), E_a is the activation energy (J/mol), R_u is the universal gas constant (8.314 J/mol K), and $T_{tumor}(x,y,z,\tau)$ is the absolute tumor temperature at a given location (x,y,z) and time instant τ. Before heating, the thermal damage index Ω is zero, it then increases with heating. 98.2% of the cells are damaged when Ω is 4. During local heating, both the blood perfusion rate and metabolism may change, responding to local temperature elevations. In this study, we assume that in the tumor region, both decrease as the local thermal damage progresses. Therefore, in the tumor, the blood perfusion rate and volumetric heat generation rate of metabolism would decrease to 1.8% of their initial values when Ω is 4, the threshold of irreversible thermal damage.

In this study, we assume that local thermal damage results in release of the intercellular fluid after rupture of cell membranes, therefore, leading to an increase in the interstitial volume fraction (porosity), φ. The relationship between local porosity and thermal damage [17,18] is described as:

$$\varphi(x,y,z,t) = \varphi_0 + (80\% - \varphi_0)\left(1 - e^{-\Omega(x,y,z,t)}\right) \quad (4)$$

where φ_0 is the tumor porosity before the heating. Eq. (4) implies that the local porosity would approach 80% after the tumor is completely damaged. This porosity value of 80% is based on an assumption that a tumor consists of cancer cells and an extracellular matrix, and the extracellular matrix volume is 20% of the total tumor volume.

Nanoparticle migration in the tumor due to heating-induced tissue damage is modeled by diffusion of nanoparticles in a porous medium [16] and the governing equation for the volume-averaged nanoparticle concentration in tissue (mol per unit volume of tissue) C is written as:

$$\frac{\partial C}{\partial t} = \nabla \bullet \left[D_n \varphi \nabla\left(\frac{C}{\varphi}\right)\right] \quad (5)$$

where D_n is the diffusion coefficient that is related to the local porosity, φ. The relationship is

$$D_n = D_{n,f}[2\varphi/(3-\varphi)] \quad (6)$$

where $D_{n,f}$ is the nanoparticle diffusion coefficient in unbound interstitial fluid [17,19]. A no-flux boundary condition at the tumor boundary is prescribed, considering that nanoparticles are unlikely to migrate to the tumor surface during the time duration of the heating.

The initial temperature fields in the tumor and mouse body are assumed uniform as 37 °C, and the initial nanoparticle concentration in the tumor region is determined from the initial Q'''_{MNH} distribution before the heating starts, obtained from our previous study [1]. We conducted simulations on five resected PC3 tumors (volume: 1261 ± 177 mm^3). As shown in our previous study [1], the total amount of the heat generation rate deposited in the tumor was approximately 0.37 W, when the tumor was subject to an alternating magnetic field at 190 kHz and 5 kA/m [1]. Consistent with our previous experimental study, the simulated heating time is selected as 25 min for later comparison to the previous experimental results.

The coupled equations (Eqs. (1)–(6)) were solved simultaneously using the multi-physics platform of COMSOL software package (version 5.2, COMSOL Inc., Stockholm, Sweden). Tissue and tumor temperature fields, thermal damage assessment, and diffusion of nanoparticles in the tumors were coupled and parameters in those equations were updated at each time step throughout the heating process of 25 min. Extremely fine tetrahedral mesh elements (550,000–770,000 tetrahedral elements in the tumor domain) were implemented to discretize the physical domain and quadratic Lagrangian elements were used to discretize the solution space. A relative tolerance of 0.001 was used for numerical convergence. A direct linear solver, MUMPS (Multifrontal Massively Parallel Sparse direct Solver) with a default pre-ordering algorithm was used for solving the temperature and concentration fields. The Backward Difference Formula (BDF) was used for time marching. The Newton-Raphson algorithm in the direct solver was used for iteration. The temporal resolution was selected as 0.01 s. The dependences on time steps and mesh sizes were studied. It was shown that doubling the total number of the mesh elements and/or halving the time step would result in less than 1% changes in the obtained temperatures and nanoparticle volume calculations. Since the simulation requires a large memory for storing the data, the entire simulation required 8–10 h on a personal computer.

3. Results

Table 1 gives the thermal and physiological properties used in the model. The tissue-dependent values of the frequency factor and activation energy are listed in Table 2. The initial tumor porosity is 0.2, and the associated nanoparticle diffusion coefficient is $9.57^{*}10^{-12}$ (m^2/s), both were obtained from previous studies [17]. Note that the initial blood perfusion rates of the tumor and the mouse body were determined

Table 1
Thermal and physiological properties used in the simulations.

	Tissue	Tumor	Blood
Thermal conductivity, k, W/mK	0.5	0.5	0.55
Density, ρ, kg/m^3	1060	1060	1060
Specific heat, c, J/kgK	3780	3780	3780
Initial blood perfusion, ω_0, 1/s	0.00285	0.00111	–
Initial metabolism, $Q'''_{met,\ 0}$, W/m^3	9265	3602	–
Initial porosity, φ_0	–	20%	–
Initial nanoparticle diffusion coefficient in interstitial fluid, $D_{n,0}$, m^2/s	–	$9.57*10^{-12}$	–

Table 2
Arrhenius kinetic coefficients used in this study.

Parameter	Symbol	Mouse tissue	PC3 tumor
Activation energy, [Jmole^{-1}]	E_a	$1.38*10^5$	$2.32*10^5$
Frequency factor, [s^{-1}]	A	$6.36*10^{19}$	$1.19*10^{35}$

from our previous experimental studies [4]. Table 3 provides the results of the sensitivity studies on the mesh size in one tumor model. As shown in Table 3, the calculation of the total nanoparticle distribution volume value is affected by the mesh size, however, as the mesh sizes are getting smaller, a convergence is evident, showing less than 1% changes in the value of the nanoparticle distribution volume. Table 3 also provides the maximal, the minimal, and the average temperature values in this tumor as affected by the mesh size, and less than 1% changes in the temperatures are shown when the total number of the mesh elements is doubled from 220 K to 570 K.

Fig. 2 shows the central slice of the 3-D temperature contours at various time instants during heating in one of the five tumors. After heating of 25 min, the maximal temperature of 75.6 °C occurs at the vicinity of the tumor center, while the minimal temperature of 54.7 °C occurs at the interface between the tumor and the mouse body. Temperature elevations in five tumors are similar, with the maximal temperature as 79.2 ± 5.2 °C (mean ± SD, n = 5) and the minimal temperature as 52.3 ± 2.4 °C (mean ± SD, n = 5), at the end of the heating duration.

The central slice of the 3-D distribution of the Arrhenius integral, Ω in one tumor, is illustrated in Fig. 3. The irreversible thermal damage, defined as $\Omega \geq 4$, is indicated by the dark red color. Thermal damage starts from the region initially occupied by the nanoparticles, then propagates to the tumor periphery. The enlargement of the damaged tumor region accelerates in the later heating time. At the end of the heating session, it is evident that the entire tumor is permanently damaged.

The spatially and temporally varying porosity distribution is shown in Fig. 4. Initially, the porosity is uniform everywhere as 20%, and it gradually increases as thermal damage spreads from the tumor center to tumor periphery. After heating for 6.7min (400 s), the porosity in most of the tumor region remains as 20%, except at the tumor center. After 10 min (600 s) of heating, the porosity at the center approaches 80% while the porosity at the tumor periphery reaches 60%. At the end of the heating session of 25 min (1500 s), the porosity of the entire tumor region is approximately 80%, suggesting permanent thermal damage, corroborating that in Fig. 3. The effective nanoparticle diffusion coefficient increases following a similar trend (Eq. (5)) during heating. The effective diffusion coefficient, D_n, increases fivefold, from its initial value of $9.57*10^{-12}$ (m^2/s) to $4.87*10^{-11}$ (m^2/s) in the entire tumor after 25 min of heating.

The transient nanoparticle concentration distribution has been simulated based on the varying porosity and nanoparticle diffusion coefficient, and the results are shown in Fig. 5. The initial nanoparticle concentration profile resembles that of the volumetric heat generation rate, with the maximal concentration as 2300 mol/m^3 on the central slice of the tumor. With the thermal damage spreading towards the tumor periphery, significant nanoparticle diffusion occurs in the regions with large concentration gradients. As a result, it is observed that nanoparticles have diffused to low concentration regions, expanding the tumor region containing nanoparticles at the end of the heating session. However, since the majority of the nanoparticles are injected at the tumor center, significant diffusion to the tumor surface is not observed in Fig. 5. As shown in Eq. (5), the volumetric heat generation rate Q'''_{MNH} is proportional to the local nanoparticle concentration, thus, Q'''_{MNH} distribution in the tumor follows a similar trend in Fig. 5.

Fig. 6 illustrates nanoparticle distribution volumes in individual concentration ranges. It is noted that the percentage of the concentration ranges shown in Fig. 6 are calculated from the maximal nanoparticle concentration in each tumor before the heating. The concentration ranges shown in Fig. 6 are selected to be consistent with our previous experimental data of nanoparticle deposition using microCT analysis [1]. The patterned bars represent the nanoparticle distribution volumes before and after heating of 25 min. The nanoparticle distribution volumes in the highest concentration range of 45%–100% decrease from the initial 44.2 ± 16.7 mm^3 to 23.7 ± 17.6 mm^3 (n = 5), in contrast to the volume increases in the lower concentration ranges. In the concentration ranges of 34%–45%, 21–34%, and 10%–21%, the average nanoparticle distribution volumes after heating increase by 28%, 78%, and 54%, respectively, from their initial values. The overall trend of nanoparticle migration from high concentration regions to low concentration regions agrees very well with our experimental data obtained by microCT analyses of resected and scanned PC3 tumors [1].

Table 3
Sensitivity of simulated results on the mesh size.

Mesh	No. of tetrahedral elements	No. of triangular elements	No. of edge elements	Nanoparticle distribution volume (mm^3)	T_{max} (°C)	T_{min} (°C)	T_{avg} (°C)
Mesh 1	5199	2048	894	188.195	74.40	44.77	58.89
Mesh 2	11,391	3466	1209	160.737	74.58	44.71	59.11
Mesh 3	19,908	5240	1530	162.734	75.23	44.90	59.81
Mesh 4	28,768	6294	1717	149.903	75.52	45.78	59.39
Mesh 5	43,635	8382	2020	206.169	75.81	45.88	60.65
Mesh 6	64,443	11,528	2423	155.446	76.27	45.81	60.50
Mesh 7	67,067	18,284	3072	153.969	76.41	45.83	60.59
Mesh 8	222,555	30,892	4148	146.089	76.43	45.82	60.56
Mesh 9	286,882	33,110	4301	144.801	76.48	45.85	60.59
Mesh 10	576,474	63,248	6133	145.591	76.51	45.84	60.62
Mesh 11	590,128	48,142	5287	142.239	76.50	45.84	60.63
Mesh 12	612,455	64,052	6156	138.863	76.48	45.83	60.60
Mesh 13	733,803	66,030	6195	137.626	76.49	45.84	60.61
Mesh 14	865,492	68,650	6278	137.380	76.49	45.84	60.61
Mesh 15	967,705	70,078	6313	137.350	76.49	45.84	60.61
Mesh 16	1,066,639	71,740	6357	137.353	76.49	45.84	60.61
Mesh 17	1,123,155	72,376	6358	137.258	76.49	45.84	60.61

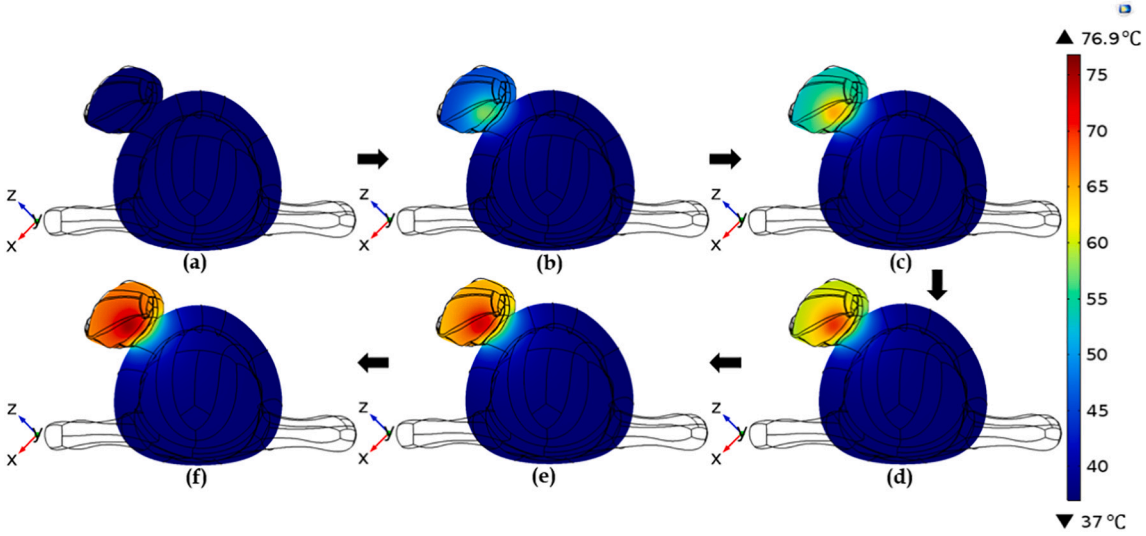

Fig. 2. The central slice of the 3-D temperature contours at various time instants during heating in one tumor: (a) $t = 0$ s; (b) $t = 300$ s; (c) $t = 600$ s; (d) $t = 900$ s; (e) $t = 1200$ s; and (f) $t = 1500$ s.

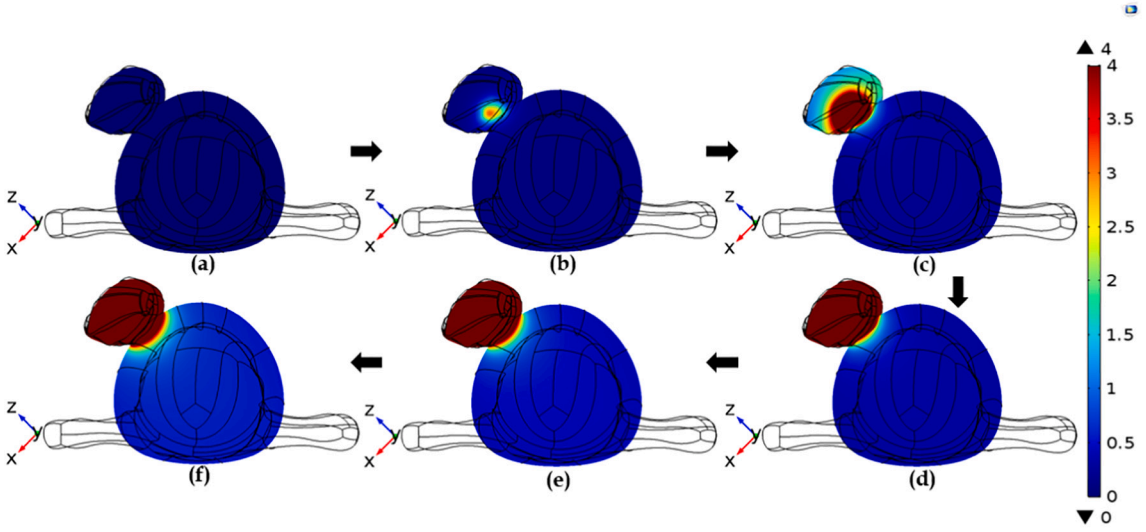

Fig. 3. The central slice of the simulated thermal damage (Ω) propagation of a tumor during heating: (a) $t = 0$ s; (b) $t = 300$ s; (c) $t = 600$ s; (d) $t = 900$ s; (e) $t = 1200$ s; and (f) $t = 1500$ s.

One could define the nanoparticle distribution volume in the entire tumor as a region containing a nanoparticle concentration $\geq 10\%$ of the maximal nanoparticle concentration, illustrated by the two solid bars on the far right in Fig. 6. The initial nanoparticle distribution volume in the entire tumor is approximately 132 ± 25 mm^3 ($n = 5$), similar to that obtained in our previous experimental data of nanoparticle deposition using microCT [1]. However, a heating of 25 min results in an increase in the nanoparticle distribution volume by approximately 21%, to 160 ± 7 mm^2 ($n = 5$). This is expected since the nanoparticles in high concentration regions would spread to low concentration regions, resulting in an enlarged distribution volume.

The initial nanoparticle distribution volume varies from one tumor to another (132 ± 25 mm^3, $n = 5$). The percentage of nanoparticle distribution volume is defined as the distribution volume in a specific concentration range (the patterned bar in Fig. 6) divided by the total nanoparticle distribution volume (the solid bar in Fig. 6). As shown in Fig. 7, the percentage of nanoparticle distribution volume in the highest concentration range decreases from the initial 32.5% to 16.9% after the heating, while in the lowest concentration range, it increases from the initial 33.8% to 58.3% after a heating of 25 min. Statistically significant differences between the initial values and the values after heating are shown in Fig. 7 in three of the four nanoparticle concentration ranges, i.e., 10%–21%, 21%–34%, and 45%–100%, based on the calculated p values using the Student t-test.

The current simulations were conducted in five generated tumor models. The simulations allow comparison of the nanoparticle volume after heating of 25 min to its initial value, i.e. before the heating in the same tumor. As shown in the patterned bars in Fig. 8, the nanoparticles originally in the highest concentration range possibly migrate to lower concentration locations, and the average particle volume in this range decreases by 43%. However, particle volumes from all the lower concentration ranges increase significantly, 28%–78% higher than the values before the heating. MicroCT analyses of resected tumors in our previous experimental study [1] are compared to the simulation predictions in the current study. Note that in the previous experiments, our microCT system did not allow in vivo animal imaging to scan the same tumor twice (before and after heating). Instead, PC3 tumors were divided into two groups: one group of 9 tumors without heating and the

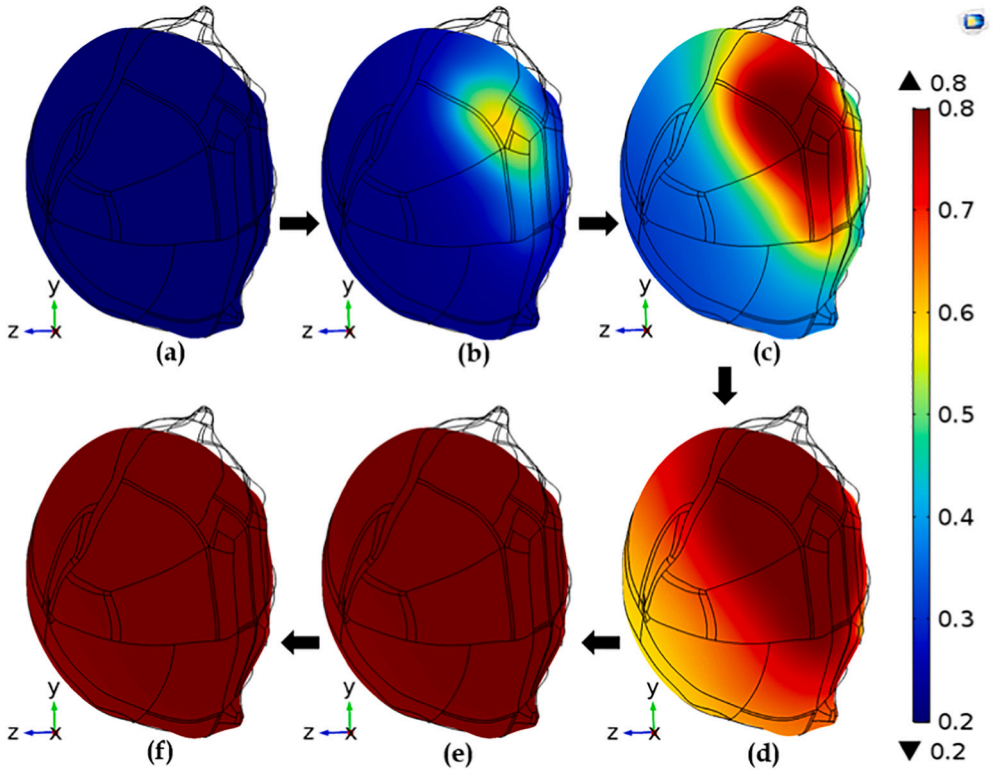

Fig. 4. The tissue porosity on the central slice of the tumor during heating: (a) $t = 0$ s; (b) $t = 200$ s; (c) $t = 400$ s; (d) $t = 600$ s; (e) $t = 800$ s; and (f) $t = 1500$ s.

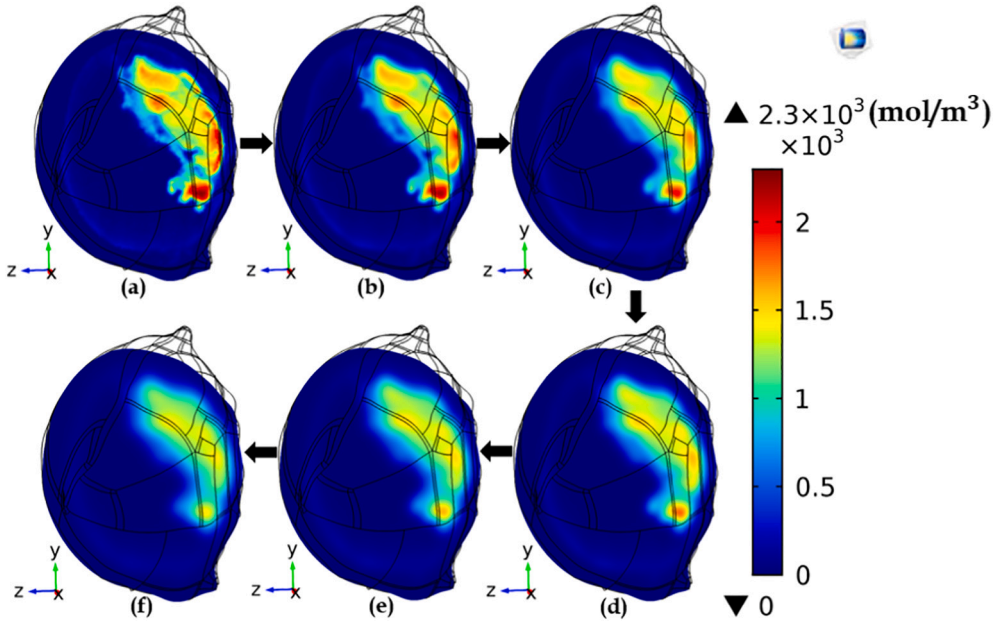

Fig. 5. Migration of nanoparticles during heating showed by the central slice of the 3-D nanoparticle concentration contours at various time instants: (a) $t = 0$ s; (b) $t = 300$ s; (c) $t = 600$ s; (d) $t = 900$ s; (e) $t = 1200$ s; and (f) $t = 1500$ s.

other group of 12 tumors subjected to heating of 25 min [1]. The solid bars in Fig. 8 illustrate the percentage change of nanoparticle volumes of the tumors with heating of 25 min to that without heating. The comparison demonstrates similar percentage changes in our previous experimental study to the simulation results of the current study. A good agreement of the trends and the orders of magnitude of the percentage change between the theoretical predictions and experimental observations lends some credibility to the current theoretical predictions.

4. Discussion

Quantitative characterization of nanoparticle transport in tissue is often difficult due to the opaque nature of the tissue and insufficient techniques to quantify its concentration distribution. Recent imaging techniques such as microCT allow visualization of nanoparticles present in tumors, however, real-time monitoring of dynamic nanoparticle migration is often not feasible. Mathematical simulation, on the other

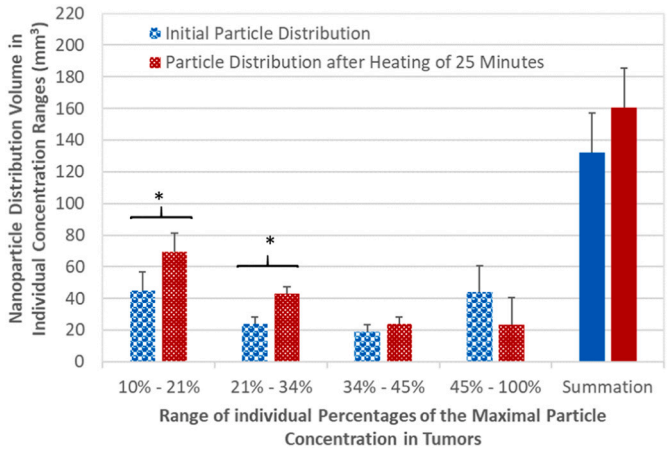

Fig. 6. Nanoparticle distribution volumes in individual particle concentration ranges in tumors before the heating (the left patterned bars) and after heating of 25 min (the right patterned bars). The solid bars on the far right side of the figure show the total nanoparticle distribution volume from 10%–100%, which is the volume summation of all the individual ranges. The p values are determined via comparing the initial values and the values after heating of 25 min. * denotes that $p < 0.05$, implying statistically significant differences between the two groups.

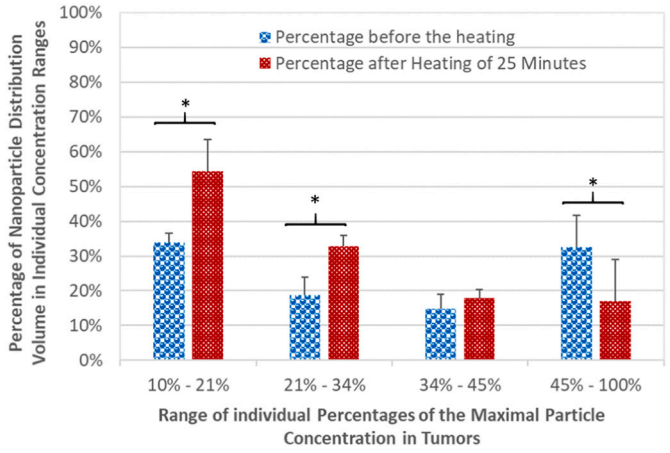

Fig. 7. Percentages of nanoparticle distribution volumes in individual particle concentration range in tumors before the heating (the left bars) and after heating of 25 min (the right bars). The p values are determined via comparing the initial values and the values after heating of 25 min. * denotes that $p < 0.05$, implying statistically significant differences between the two groups.

hand, provides a useful tool to isolate various transport mechanisms and to evaluate contributions of individual factors. In this study, we evaluate one of the mechanisms that have potential to cause nanoparticle migration from their original locations. We have demonstrated that nanoparticle diffusion from high concentration regions to low concentration regions is significant with enhancements in porosity and diffusion coefficient, caused by irreversible thermal damage in tumors. Theoretically, the diffusion (migration) distance L over a duration of t is proportional to the square root of the diffusion coefficient and time, i.e., $L \sim \sqrt{D_n t}$. Based on the diffusion coefficient of $9.57*10^{-12}$ m^2/s in tumors before heating, L could be approximately 0.12 mm after 25 min. Due to thermal damage, the enhanced diffusion coefficient is enhanced to $4.87*10^{-11}$ (m^2/s), leading to a diffusion distance as 0.27 mm. Since the feature size of the initial nanoparticle distribution volume is approximately 130 mm^3, such an increase by diffusion is not trivial.

The theoretical predictions of temperature elevations by the coupled model agree well with that in previous theoretical and experimental

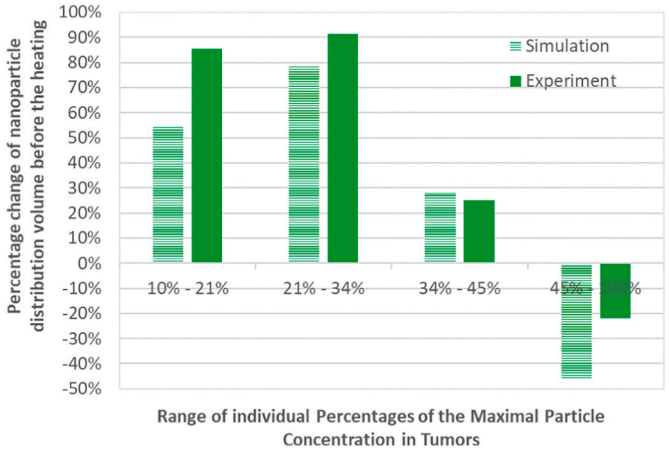

Fig. 8. Percentage change in the nanoparticle volume in individual particle concentration ranges from its value before the heating. The bars on the left represent the simulation results of the nanoparticle volume after heating of 25 min from its value before the heating. The bars on the right represent experimental results of previous microCT analyses of resected tumors [1].

results [11–13,20]. Those previous theoretical simulations were used to design heating protocols to adequately damage the entire tumors. We implemented a designed heating protocol to PC3 tumors implanted in mice [20]. Histological analyses of the resected tumors after heating illustrated vast regions of apoptotic and necrotic cells, consistent with the regions of significant temperature elevations [20]. Longitudinal studies to measure tumor shrinkage were also performed for tracking tumor sizes for 8 weeks post heating [20]. The treated tumors with 25 min of heating disappeared after only a few days and the disappearance were maintained for 8 weeks, suggesting accuracy of the simulation. Further, the current simulation demonstrates a decrease in the nanoparticle distribution volume in the highest concentration range, while increases in the lower concentration ranges. This trend agrees very well with our microCT imaging analyses [1]. Future experimental studies are warranted to using real-time imaging tools to monitor porosity changes caused by local heating.

The current study is limited by not taking into consideration transport behavior of individual nanoparticles and nanoparticle interactions with the cells and the extracellular matrix, rather, nanoparticles are modeled as molecular diffusion from high to low concentration regions. This approach neglects particle motions driven by multiple forces acting on a particle, including van der Waals attractive force, electrostatic double layer force, and drag and lift forces [21]. Nanoparticles may be trapped on the solid extracellular matrix of tissue, therefore, even if those nanoparticles are highly concentrated, the diffusion induced force (Brownian motion) may not be able to overcome other forces to trigger the initial move. To accurately model the motions of individual nanoparticles, a microscale trajectory tracking model may be needed to follow movements of nanoparticles, and the tracking model could then be implemented in a macroscale model to simulate the field of nanoparticle concentration, as shown in previous studies [21,22].

In this study, we use the Pennes bioheat equation to simulate the temperature field in tissues. Pennes bioheat equation is a continuum model, in which the effect of blood flow in the region of interest is averaged over a control volume. Thus, in the considered tissue region, there is no blood vessel present; however, its thermal effect is treated by either adding an additional term in the conduction equation for the tissue or changing some of the thermal/physical parameters in the conduction equation. In addition to the Pennes bioheat equation, other research groups also attempted to develop better continuum models to accurately quantify thermal effect of blood perfusion on tissue temperatures [23–25]. One thing that is not clear from those models is the calculation of the “to-be-determined” parameters appearing in those

equations. The determination of those parameters still requires development of a blood vessel-tissue unit for establishing the relationship to the specific vasculature and blood perfusion rate. Therefore, those continuum models have not received the same popularity as that received by the Pennes bioheat equation. Despite its simplicity and shortcomings, the Pennes bioheat equation, which requires only a local perfusion rate and an arterial blood temperature as inputs, is relatively easy to use without detailed anatomical knowledge of the tissue vasculature. Furthermore, tables of blood perfusion rates in various tissues/organs are conveniently available in the literature.

The above continuum bioheat transfer models assume an infinite speed of propagation of the thermal wave through tissue. Some research groups suggest that a non-Fourier damped wave model would be more appropriate to account for the finite speed of propagation of heat waves. Several research groups have implemented a non-Fourier wave term to the Pennes bioheat equation to simulate temperature elevations in tissue [26–29]. Unfortunately, experimental data of the required time constant appearing in the equation are limited. So far, this approach has only been used in hyperthermia treatment when laser heating is involved. Those previous studies suggest that the time constant may be approximately between 5 and 15 s. It is possible that the non-Fourier term would become significant when the heating rate is very high, as in laser related heating processes. Future simulations may be needed to evaluate the effect of including thermal waves in those continuum bioheat models in magnetic nanoparticle hyperthermia applications.

Another limitation of this study is that several other transport mechanisms were not modeled in the simulation [30]. We did not model the advection of fluid from the tumor center to the periphery. Fluid extravasation from a capillary to its surrounding interstitial space is a continuous process due to leaky capillaries in tumors. The fluid has to be removed by the lymphatic system to establish a steady state. Most solid tumors have poorly developed lymphatic vessels, leading to a high interstitial fluid pressure built up at the tumor center. Lymphatic vessels typically contract when the temperature is reduced and dilate when the temperature is elevated. It is possible that local heating might improve lymphatic drainage. If local heating results in opening of the originally collapsed lymphatic vessels, the advection of fluid from the tumor center to periphery might become stronger during heating. Therefore, nanoparticles in the interstitial tissue space might be carried away by the bulk interstitial fluid to the tumor periphery. Another possible mechanism is the increase in local blood perfusion rate in tumors at the beginning of a local heating. It is well known that during local heating, local blood perfusion rate may increase initially, then decrease later due to damage to the vasculature [31,32]. A larger amount of blood delivered to tumors should increase the pressure in the capillaries in tumors, causing more fluid extravasation. This mechanism together with improved lymphatic drainage would further induce nanoparticle migration from the central region to the tumor periphery [30]. Future theoretical simulations and experimental measurements are needed to evaluate the contribution of those mechanisms, and to validate theoretical predictions.

The current theoretical simulation was carried out by the multiphysics platform in the COMSOL software package. Since the simulation domain used generated tumor models from microCT scans of resected tumors, singularities occurred during meshing, even after the tumor surface was smoothed out. As shown in Fig. 1, the nanoparticle occupied region required very fine meshes to simulate the diffusion process. The finalized mesh setting in this study was sufficient for the heat transfer simulation, as doubling the total number of elements would result in less than 0.1 °C in the temperature fields. On the other hand, the diffusion process is more sensitive to the mesh size than the heat transfer process, shown in Table 3. In this study, we pushed the limit of the memory of the computer. It was demonstrated that the finalized mesh size would not cause changes of more than 1% in the particle distribution volume, when the total number of mesh elements was doubled. Although a finer mesh might be ideal to continue to improve the accuracy of the simulation of the diffusion process, it would require much longer computational time, and yet, it would not change the conclusions drawn from this study.

This research may be beneficial to targeted drug delivery using nanocarriers. Unlike hyperthermia treatment, success of drug delivery relies on whether all the tumor cells are subjected to a minimal level of drug concentration. Anti-cancer drugs are often delivered to targeted tumors via intravenous injections. The difficulty faced is how to deal with poorly perfused tumors and/or high interstitial tumor pressures. Enhancement in diffusion coefficient in the interstitial space in tumors by heating would facilitate dispersion of nanocarriers/drugs to the entire tumor. In other words, it would result in a more uniform drug concentration. Nanoparticle diffusion from a high concentration region to a low concentration region is governed by the diffusion coefficient. The diffusion (migration) distance L is typically proportional to the square root of the diffusion coefficient and time. Therefore, the smaller the diffusion coefficient is, the longer it takes to achieve the same migration distance. In the current study, the diffusion coefficient increases by five folds during the heating. Increasing D_n by five folds would enhance the migration distance by 2.3 folds. This would have significant effects on nanoparticle transport in tumors. In a systemic delivery of nanoparticles to tumors, nanoparticles pass through the pores in tumor capillary walls and then diffuse in the interstitial fluid space. If the diffusion distance with the initial D_n is 10 μm, the enhancement in D_n due to local heating would have been 23 μm. This would be significant to improve nanoparticle penetration in the interstitial space since a typical capillary to capillary distance in tumors is approximately 50–100 μm [33]. Therefore, mild or modest hyperthermia using magnetic nanoparticles as therapeutic agent carriers can achieve dual treatment efficacies via thermal damage and enhancement in uniform drug delivery.

In summary, a theoretical framework consisting of a nanoparticle diffusion model and a heat transfer model was developed to examine possible nanoparticle redistribution mechanisms in magnetic nanoparticle hyperthermia. The simulation results demonstrate the importance of including dynamic interactions among heat transfer, thermal damage, and nanoparticle migration in the model for nanoparticle hyperthermia applications. The simulated temperature elevations in tumors are similar to that in previous studies. The theoretical predictions of nanoparticle migration from a high concentration region to a low concentration region agree well with experimental results of microCT scan analyses. It is concluded that thermal damage-induced enhancement in nanoparticle diffusion may be one of the mechanisms to explain nanoparticle migration during magnetic nanoparticle hyperthermia. It also suggests a feasibility of enhancing nanoparticle dispersion from injection sites using deliberate thermal damage.

Declaration of Competing Interest

The authors declare that they have no known competing financial interests or personal relationships that could have appeared to influence the work reported in this paper.

Acknowledgements

This research was supported by an NSF research grant (CBET-1705538). The research was performed in partial fulfilment of the requirements for the Ph.D. degree by Manpreet Singh from the University of Maryland Baltimore County, Baltimore, Maryland, USA.

References

[1] Q. Gu, T. Joglekar, C. Bieberich, R. Ma, L. Zhu, Nanoparticle redistribution in PC3 tumors induced by local heating in magnetic nanoparticle hyperthermia: In vivo experimental study, ASME J. Heat Transf. 141 (3) (2019) 1–9, https://doi.org/10.1115/1.4042298, 032402.

[2] M. Singh, T. Singh, S. Soni, Pre-operative assessment of ablation margins for variable blood perfusion metrics in a magnetic resonanace imaging based complex breast tumour anatomy: simulation paradigms in thermal therapies, Comp.

Methods Programs Med. 198 (2021) 105781, https://doi.org/10.1016/j.cmpb.2020.105781.
[3] M. Singh, Medical Imaging Assisted Computational Bio-Heat Transfer Analysis of Magnetic Nanoparticles Induced Hyperthermia for Breast Cancer, M.S. Thesis, Thapar Institute of Engineering and Technology University, Patiala, Punjab, India, 2016. http://hdl.handle.net/10266/4116.
[4] M. Singh, Q. Gu, R. Ma, L. Zhu, Heating protocol design affected by nanoparticle redistribution and thermal damage model in magnetic nanoparticle hyperthermia for cancer treatment, ASME J. Heat Transf. 142 (7) (2020) 072501–072510, https://doi.org/10.1115/1.4046967.
[5] M. Johannsen, A. Jordan, R. Scholz, M. Koch, M. Lein, S. Deger, J. Roigas, K. Jung, S. Loening, Evaluation of magnetic fluid hyperthermia in a standard rat model of prostate cancer, J. Endourol. 18 (5) (2004) 495–500, https://doi.org/10.1089/0892779041271715.
[6] M. Johannsen, U. Gneveckow, L. Eckelt, A. Feussner, N. Waldöfner, R. Scholz, S. Deger, P. Wust, S.A. Loening, A. Jordan, Clinical hyperthermia of prostate cancer using magnetic nanoparticles: presentation of a new interstitial technique, Int. J. Hyperth. 21 (7) (2005) 637–647, https://doi.org/10.1080/02656730500158360.
[7] M. Johannsen, U. Gneveckow, K. Taymoorian, B. Thiesen, N. Waldöfner, R. Scholz, K. Jung, A. Jordan, P. Wust, S.A. Loening, Morbidity and quality of life during thermotherapy using magnetic nanoparticles in locally recurrent prostate cancer: results of a prospective phase I trial, Int. J. Hyperth. 23 (3) (2007) 315–323, https://doi.org/10.1080/02656730601175479.
[8] A. Jordan, R. Scholz, P. Wust, H. Fahling, J. Krause, W. Wlodarczyk, B. Sander, T. Vogl, R. Felix, Effects of magnetic fluid hyperthermia (MFH) on C3H mammary carcinoma in vivo, Int. J. Hyperth. 13 (6) (1997) 587–605, https://doi.org/10.3109/02656739709023559.
[9] K. Maier-Hauff, R. Rothe, R. Scholz, U. Gneveckow, P. Wust, B. Thiesen, A. Feussner, A.V. Deimling, N. Waldoefner, R. Felix, A. Jordan, Intracranial thermotherapy using magnetic nanoparticles combined with external beam radiotherapy: results of a feasibility study on patients with glioblastoma multiforme, J. Neuro-Oncol. 81 (2007) 53–60, https://doi.org/10.1007/s11060-006-9195-0.
[10] L. Du, J. Zhou, X. Wang, L. Sheng, G. Wang, X. Xie, G. Xu, L. Zhao, Y. Liao, J. Tang, Effect of local hyperthermia induced by nanometer magnetic fluid on the rabbit VX2 liver tumor model, Prog. Nat. Sci. 19 (12) (2009) 1705–1712, https://doi.org/10.1016/j.pnsc.2009.06.006.
[11] A. Attaluri, R. Ma, Y. Qiu, W. Li, L. Zhu, Nanoparticle distribution and temperature elevations in prostatic tumors in mice during magnetic nanoparticle hyperthermia, Int. J. Hyperth. 27 (5) (2011) 491–502, https://doi.org/10.3109/02656736.2011.584856.
[12] M. Singh, R. Ma, L. Zhu, Theoretical evaluation of temperature elevation, thermal damage, tumor porosity enhancement, and magnetic nanoparticle migration in tumors during local heating, in: Summer Biomechanics, Bioengineering and Biotransport Conference, Seven Springs, PA, USA, 2019. June 25–28. (Paper number SB3C-2019-105).
[13] A. LeBrun, R. Ma, L. Zhu, MicroCT image based simulation to design heating protocols in magnetic nanoparticle hyperthermia for cancer treatment, J. Therm. Biol. 62 (Pt. B) (2016) 129–137, https://doi.org/10.1016/j.jtherbio.2016.06.025.
[14] H.H. Pennes, Analysis of tissue and arterial blood temperatures in the resting human forearm, J. Appl. Physiol. 1 (2) (1948) 93–122, https://doi.org/10.1152/jappl.1948.1.2.93.
[15] I.A. Chang, U.D. Nguyen, Thermal modeling of lesion growth with radiofrequency ablation devices, Biomed. Eng. Online 3 (1) (2004) 27, https://doi.org/10.1186/1475-925X-3-27.
[16] G.A. Truskey, F. Yuan, D.F. Katz, Transport Phenomena in Biological Systems, Second ed., Prentice Hall, Upper Saddle River, New Jersey, 2009.
[17] A. Zhang, X. Mi, G. Yang, L.X. Xu, Numerical study of thermally targeted liposomal drug delivery in tumor, J. Heat Transf. 131 (4) (2009) 043209–043219, https://doi.org/10.1115/1.3072952.
[18] S.H. Jang, M.G. Wientjes, D. Lu, J.L.-S. Au, Drug delivery and transport to solid tumors, Pharm. Res. 20 (2003) 1337–1350, https://doi.org/10.1023/A:1025785505977.
[19] A.W. El-Kareh, S.L. Braunstein, T.W. Secomb, Effect of cell arrangement and interstitial volume fraction on the diffusivity of monoclonal antibodies in tissue, Biophys. J. 64 (5) (1993) 1638–1646, https://doi.org/10.1016/S0006-3495(93)81532-7.
[20] A. LeBrun, T. Joglekar, C. Bieberich, R. Ma, L. Zhu, Treatment efficacy for validating microCT based theoretical simulation approach in magnetic nanoparticle hyperthermia for cancer treatment, ASME J. Heat Transf. 139 (1–7) (2017) 051101.
[21] D. Su, R. Ma, L. Zhu, Numerical study of nanofluid infusion in deformable tissues for hyperthermia cancer treatment, Med. Biol. Eng. Comput. 49 (2011) 1233–1240, https://doi.org/10.1007/s11517-011-0819-y.
[22] R. Ma, D. Su, L. Zhu, Multiscale simulation of nanoparticle transport in deformable tissue during an infusion process in hyperthermia treatments of cancer, in: W. J. Minkowycz, E. Sparrow, J.P. Abraham (Eds.), Nanoparticle Heat Transfer and Fluid Flow, Computational & Physical Processes in Mechanics & Thermal Science Series 4, CRC Press, Taylor & Francis Group, Boca, Raton, FL, 2012.
[23] S. Weinbaum, L. Jiji, A new simplified bioheat equation for the effect of blood flow on local average tissue temperature, ASME J. Biomech. Eng. 107 (2) (1985) 131–139.
[24] D. Shrivastava, J.T. Vaughan, A generic bioheat transfer thermal model for a perfused tissue, ASME J. Biomech. Eng. 131 (7) (2009), 074506.
[25] A. Nakayama, F. Kuwahara, A general bioheat transfer model based on the theory of porous media, Int. J. Heat Mass Transf. 51 (11–12) (2008) 3190–3199.
[26] A. Banerjee, A. Ogale, C. Das, K. Mitra, C. Subramanian, Temperature distribution in different materials due to short pulse laser irradiation, Heat Transf. Eng. 26 (2005) 41–49.
[27] K.E. Glass, M.N. Ozisik, D.S. McRae, B. Vick, Hyperbolic heat conduction with temperature-dependent thermal conductivity, J. Appl. Phys. 59 (1986) 1861–1865.
[28] A. Vedavarz, K. Mitra, S. Kumar, Hyperbolic temperature profiles for laser surface interactions, J. Appl. Phys. 76 (1994) 5014–5021.
[29] M. Jaunich, S. Raje, K. Kim, K. Mitra, Z. Guo, Bio-heat transfer analysis during short pulse laser irradiation of tissues, Int. J. Heat Mass Transf. 51 (2008) 5511–5521.
[30] M. Singh, R. Ma, L. Zhu, Theoretical evaluation of enhanced gold nanoparticle delivery to PC3 tumors due to increased hydraulic conductivity or recovered lymphatic function after mild whole body hyperthermia, Med. Biol. Eng. Comput. 59 (2021) 301–313, https://doi.org/10.1007/s11517-020-02308-4.
[31] X. He, S. McGee, J.E. Coad, F. Schmidlin, P.A. Iaizzo, D.J. Swanlund, S. Kluge, E. Rudie, J.C. Bischof, Investigation of the thermal and tissue injury behaviour in microwave thermal therapy using a porcine kidney model, Int. J. Hyperth. 20 (6) (2004) 567–593.
[32] X. He, Thermostability of biological systems: fundamentals, challenges, and quantification, Open Biomed. Eng. J. 5 (1) (2011) 47–73.
[33] J.W. Baish, T. Stylianopoulos, R.M. Lanning, W.S. Kamoun, D. Fukumura, L. L. Munn, R.K. Jain, Scaling rules for diffusive drug delivery in tumor and normal tissues, PNAS 108 (5) (2011) 1799–1803, https://doi.org/10.1073/pnas.1018154108.